

# MODELING OF COMPOSITE ACTION IN CONCRETE-FILLED STEEL TUBES USING COUPLED RBSM AND SHELL FEM

Rodolfo P. MENDOZA Jr<sup>\*1</sup>, Yoshihito YAMAMOTO<sup>\*2</sup>, Hikaru NAKAMURA<sup>\*3</sup> and Taito MIURA<sup>\*4</sup>

## ABSTRACT

Three types of interface models for concrete-steel interaction in concrete-filled steel tube (CFST) were quantitatively and qualitatively investigated using published test results. The study is part of the development of a coupled rigid body spring model (RBSM) and shell finite element method (FEM) aimed at modeling CFST and similar concrete-steel composites by utilizing the suitable numerical method for each material, i.e., RBSM for concrete and shell FEM for steel tube. The results of the investigation were discussed and the most appropriate interface model was selected.

**Keywords:** RBSM, shell FEM, concrete-filled steel tube, interface element, composite

## 1. INTRODUCTION

The use of steel jacket as a retrofit method for strength-deficient RC column provides an effective passive confinement which increases the strength and ductility of the member. The interaction of concrete and steel tube, however, is not merely a superposition of their individual behavior but rather includes a complex interface interaction. Currently, there is no uniform standard on how to account the bond in such composite which may be due to the varying experimental test results on the bond behavior of these systems [1, 2]. The behavior of a steel jacketed RC column is more or less similar to that of a concrete-filled steel tube (CFST). Several numerical formulations have been already introduced to model such system and most of these methods are based on finite or fiber element techniques with nonlinear capabilities. Modeling of concrete-steel interface varies greatly on the type of elements used. A nine-node interface element was used by Hu et al. [3] which allow sliding and friction. In their model, the concrete and steel were allowed to be separated but impenetrability was maintained. Johansson and Gylltoft [4] supported their experimental tests with numerical models in which they utilized an eight-node and six-node finite element to model the steel and concrete, respectively. Their interface model consists of a contact pressure-overclosure model in the normal direction and a Coulomb friction-type model on tangential interfaces.

In the present study, three types of modeling approaches for concrete-steel tube interface were investigated. These are: (1) perfect shear model; (2) Mohr-Coulomb friction model; and (3) no shear (full slip) model. These interface models were investigated as part of the development of a coupled discrete and

continuum numerical method to model CFST. The discrete method is based on Rigid Body Spring Model (RBSM) which is used to model the concrete core. The method has been proven effective in modeling concrete behavior particularly in the inelastic regime. The method can well simulate softening and localization fractures of concrete such as cracking and failure behaviors of RC members [5]. The steel tube, on the other hand, is modeled as a continuum, using degenerated shell finite element. This coupled approach is introduced to capture the salient features of concrete and steel by utilizing the most appropriate numerical method for each material, i.e., RBSM for concrete and a general shell FEM for steel. Since most of the existing interface models are based on a continuum-to-continuum interface contact, an investigation of the most appropriate discrete-to-continuum interface contact is necessary. The investigation was performed by comparing simulation results of three interface models with published CFST experimental results. Both strength comparison using axial load-strain relationships and qualitative comparison using final deformed behavior of CFST were presented. The results of the investigation were discussed and the most appropriate interface model for the proposed method was selected.

## 2. CONCRETE MODELING

The RBSM developed by Kawai [6] was introduced in recognition of the limitations of continuum models particularly in modeling nonlinear behavior of materials. The term "Rigid Body" was coined based on experimental observations that when a structure reaches its ultimate state, the structure may collapse, crushed, and be separated into pieces like

\*1 Ph.D. Student, Dept. of Civil Engineering, Nagoya University

\*2 Associate Prof., Dept. of Civil Engineering, Nagoya University, Dr.E., JCI Member

\*3 Prof., Dept. of Civil Engineering, Nagoya University, Dr.E., JCI Member

\*4 Assistant Prof., Dept. of Civil Engineering, Nagoya University, Dr.E., JCI Member

rigid body [6]. This description highly depicts the behavior of concrete in the post-peak regime. The authors have already utilized RBSM in a wide application of concrete engineering problems—ranging from material (e.g., corrosion induced cracking in concrete [7], to structural member analysis (e.g., shear failure mechanism evaluation [8]), and plate analysis subjected to impact [9])—and have shown that the method can well simulate the salient features of concrete such as cracking, localization, and softening behavior.

In RBSM, concrete is modeled as an assemblage of rigid particles discretized using Voronoi diagram and interconnected by sets of normal and shear springs at predefined evaluation points as shown in Fig. 1. Contrary to continuum mechanics, in RBSM, the response of the springs dictates the interaction of the particles (elements) instead of their internal behavior. Thus, modeling of mechanical behaviors of concrete is simulated by introducing the material constitutive models into the springs (i.e., tension, compression and shear).

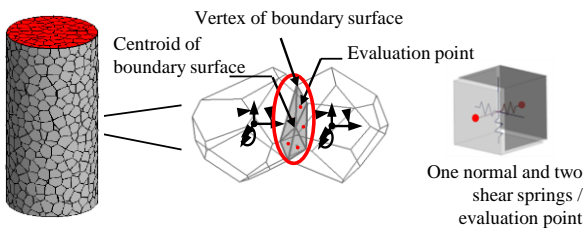


Fig.1 Concrete model as RBSM

The concrete modeling using RBSM used in this study is based on a meso-scale, single phase averaging model of concrete. Constitutive models were developed utilizing meso-scale parameters determined through experimental validations and are explained in detailed in Yamamoto et al. [5, 10].

### 3. STEEL TUBE MODELING

The steel tube is modeled using a general four-node degenerated shell element utilizing the iso-parametric coordinates as the convected coordinate system. An important feature of this element is that it is based on geometrically nonlinear shell formulation using

integrated FEM approach for total and updated Lagrangian method introduced by Noguchi and Hisada [11]. The shear locking problem commonly present in low-order shell elements was solved using selective reduced integration scheme. Material nonlinearity is based on Von Mises yield criterion with isotropic hardening. The developed program was verified using a benchmark model commonly used for geometrically nonlinear shell. Fig. 2 shows the result of verification for a cantilever with end shear force.

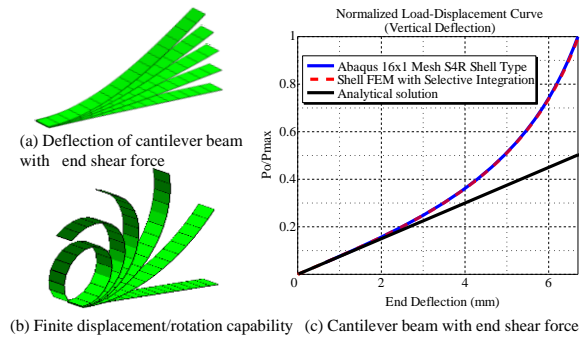


Fig. 2 Shell verification

The comparison shows the good agreement between the introduced shell and the simulated benchmark model by Sze et al. [12] using ABAQUS S4R shell type.

### 4. CONCRETE-STEEL INTERFACE MODELS

The load transfer mechanism between RBSM and shell FEM is provided by discrete interface elements pre-assigned at every shell nodes. Fig. 3(a) shows the illustration of this contact while Fig. 3(b) shows the contact points positioned at random locations on RBSM elements' surface. To preserve the contact between the two elements, i.e., between RBSM and shell, contact area is calculated by dividing the RBSM element surface equally with the number of shell nodes in contact with the surface. The relative displacement between shell node and an arbitrary contact point in the RBSM surface is defined by Eq. 1 which follows the same concept of contact introduced for beam-RBSM connection [10] and was extended to shell FEM as described below.

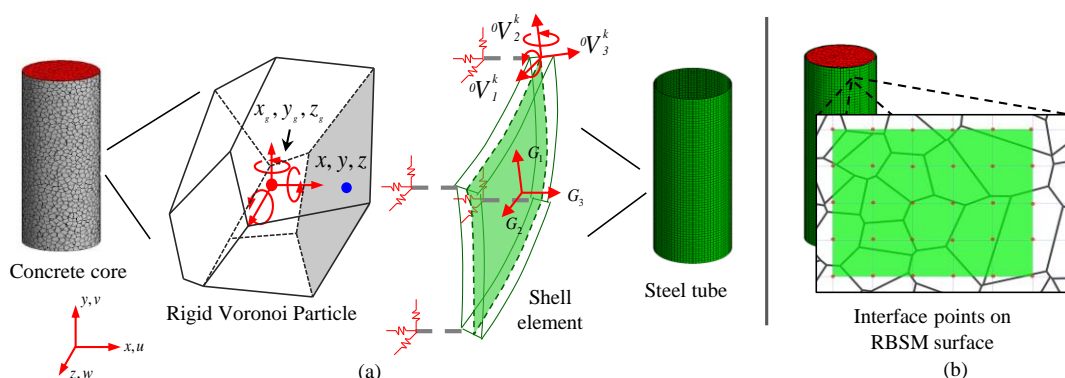


Fig.3 RBSM-shell element connection

$$\mathbf{d}_g = \mathbf{B}\mathbf{u} \quad (1)$$

where:  $\mathbf{d}_g^T = [\delta_n \ \delta_v \ \delta_c]$  are the relative displacements in the normal and tangential directions, and  $\mathbf{u}$  are the translational displacements of the shell node and displacements of the RBSM centroid defined as:

$$\mathbf{u}^T = [u_R \ v_R \ w_R \ \theta_{xR} \ \theta_{yR} \ \theta_{zR} \ u_S \ v_S \ w_S]$$

The subscripts R and S refer to RBSM and shell displacements, respectively. The  $\mathbf{B}$  matrix is defined as follows:

$$\mathbf{B} = \begin{bmatrix} -1 & 0 & 0 & 0 & -(z-z_g) & (y-y_g) & 1 & 0 & 0 \\ 0 & -1 & 0 & (z-z_g) & 0 & -(x-x_g) & 0 & 1 & 0 \\ 0 & 0 & -1 & -(y-y_g) & (x-x_g) & 0 & 0 & 0 & 1 \end{bmatrix} \quad (2)$$

The relative displacements are transformed locally using the transformation matrix  $\mathbf{R}$ , see Eqs. 3 and 4, with  $l$ ,  $m$ , and  $n$  refers to the direction cosines of shell element axis.

$$\mathbf{R} = \begin{bmatrix} l & m & n \\ -m & l & 0 \\ \frac{-nl}{\sqrt{l^2+m^2}} & \frac{-mn}{\sqrt{l^2+m^2}} & \sqrt{l^2+m^2} \end{bmatrix} \quad (3)$$

$$\mathbf{d}_l = \mathbf{R}\mathbf{d}_g \quad (4)$$

The stiffness matrix is defined using Eqs. 5.

$$\mathbf{K} = \mathbf{B}^T \mathbf{R}^T \mathbf{D} \mathbf{R} \mathbf{B} \quad (5)$$

where the D matrix is the spring constitutive matrix given as:

$$\mathbf{D} = \begin{bmatrix} \mathbf{K}_n & 0 & 0 \\ 0 & \mathbf{K}_v & 0 \\ 0 & 0 & \mathbf{K}_c \end{bmatrix} \quad (6)$$

where  $K_n$ ,  $K_v$ , and  $K_c$  are the stiffness in the normal, shear vertical and shear circumferential directions, respectively. The three types of constitutive models for interface elements investigated in this study are discussed in the following sections.

#### 4.1 Perfect Shear Model

The perfect shear model represents the full (perfect bond) composite action between concrete and steel tube. In this model, the normal and shear interface springs are assumed to be linear and independent. The normal contact allows the separation of RBSM and shell under tension state and prohibits the penetration of one element to the other. The stiffness in the normal and shear directions can be generally defined as:

$$K = EA/h \quad (7)$$

where  $E$  is taken as the concrete's elastic modulus for

normal spring and concrete's shear modulus for shear springs, while  $A$  is defined as the contact area, and  $h$  is defined as the distance from the RBSM's centroid to the shell nodes referred to the mid-surface of the shell element. The representation of the perfect shear constitutive model is shown in Fig. 4.

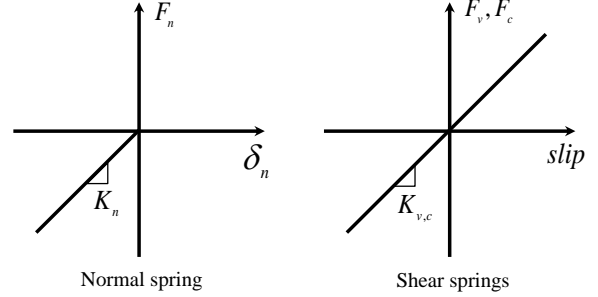


Fig.4 Perfect shear interface model

#### 4.2 Mohr-Coulomb Friction Model

The Mohr-Coulomb friction model is presented in Fig. 5. This model provides a similar linear model for normal spring but the strength of the shear springs is dependent on the magnitude of normal contact. This relationship is defined by the coefficient of friction determined as equal to 0.25 from a separate analysis. The shear spring model is a bilinear hardening model in which the hardening coefficient is taken as 1/100 of the initial shear spring's stiffness. The set of stiffness are defined the usual way using Eqs. 7. Separation of RBSM and shell element is imposed when the normal spring is under tension.

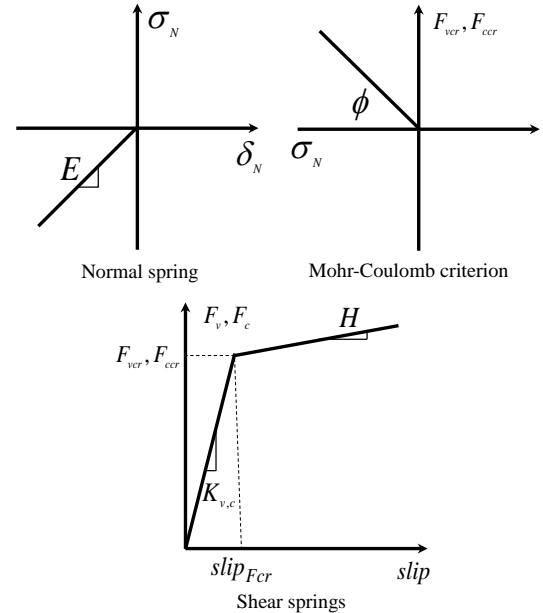


Fig.5 Mohr-Coulomb friction model

#### 4.3 No Shear (Slip) Model

The no shear or slip model assumes that no composite action occurs in the concrete-steel interface. The contact is only introduced through the normal spring when it is under compression load. Similar to perfect and Mohr-Coulomb case, the normal contact

allows the separation of the two elements under tension condition and applies the rule of element impenetrability. Similar to the two previous models, the system spring stiffness are calculated using Eqs. 7.

### 5. COMPARISON OF INTERFACE MODELS

Comparison of interface models was conducted by simulation of published experimental results of axially loaded CFST. In this study, the experiments conducted by Johansson and Gylltoff [4] were used which include CFST loading cases of concrete-only loaded (labeled as SFC), and concrete and steel loaded (labeled as SFE). The specimens were selected to provide both quantitative comparison based on axial load-strain curves, and qualitative comparison using the final deformed behavior of test specimens. The reported axial strains from test results were based on measurements obtained from vertical displacement transducer while the reported axial loads were obtained with measurements from an oil pressure gauge which was increased manually at a constant rate up to maximum load [4]. The geometric and mechanical properties of these specimens are presented in Table 1.

Table 1 Properties of simulated specimens (A)

Type	H (mm)	D (mm)	T (mm)	f'c (MPa)	fy (MPa)	Loaded section
SFE	650	159	4.8	64.5	433	CS
SFC	650	159	4.8	64.5	433	C

\*CS = concrete and steel; C = concrete; H = height; D = diameter; T = steel tube thickness; f'c = concrete's compressive strength; and fy = yield strength of steel tube.

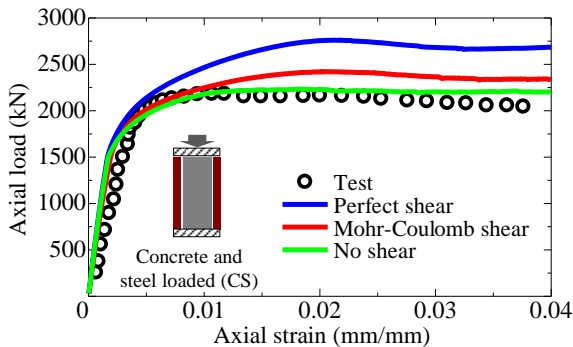


Fig.6 Axial load - strain curves for SFE

The axial load-strain results for SFE and SFC specimens are shown in Fig. 6 and Fig. 7, respectively. In each figure, the test result and the results of simulation from the three investigated interface models are presented. The simulation results for SFE specimen show the perfect shear case provides the highest estimate of axial strength while the no shear or slip case provides the lowest strength estimate. The Mohr-Coulomb friction case provides a middle ground between the perfect and no shear case. The strength predictions from the no shear case and Mohr-Coulomb case show a better agreement with the test result. In all the three cases, a plastic post-peak behavior was observed. Fig. 7 shows the comparison of axial load-strain curves for SFC. The perfect shear case and

the no shear case show almost similar peak strength, but difference in their post-peak behavior is evident with the perfect shear case shows a hardening post-peak behavior while the no shear case shows a softening response. Among the three cases, the Mohr-Coulomb friction case provides the lowest strength prediction which is also the nearest prediction to the test results. Post-peak behavior for Mohr-Coulomb case is characterized by nearly perfect plastic hardening response.

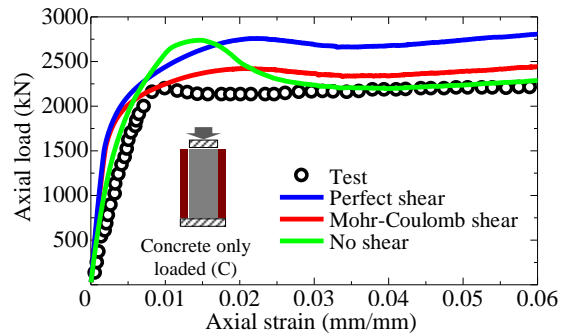


Fig.7 Axial load - strain curves for SFC

The qualitative comparison of simulated deformed behavior—with concrete and steel tube behavior shown separately—from three interface models and test results are shown in Fig. 8. These comparisons are based on the final deformed behavior of test and simulation results. For SFE specimen, the behavior of the perfect shear case and the Mohr-Coulomb case show an almost similar lateral deformation while the no shear case shows a more concentrated damage near mid-height. Better agreement with the test result can be observed from the simulated deformed behaviors of the perfect shear and Mohr-Coulomb case. On the other hand, the length of compressive failure zone of concrete tends to concentrate (or localized) at mid-height for the no shear case results relative to the two other cases. For the SFC specimen, a similar behavior can be observed for the perfect shear and Mohr-Coulomb case which show a relatively distributed damage along the specimen height. Once again, these results are in better agreement with the test result. For the no shear case, the simulated deformed behavior shows a more profound concrete damage or failure near mid-height similar to that observed for SFE specimen, the position of the localized failure with respect to the height is, however, lower than the SFE case, i.e., near the bottom part of the specimen. Concrete cracking is also more visible for SFC as this specimen sustained larger deformation than SFE specimen.

### 6. DISCUSSION OF RESULTS

The results based on the comparison of axial load-strain curves and final deformed behaviors of tests and simulation results show that by changing the interface model between concrete and steel—in this case between RBSM and shell FEM—the composite action of CFST also changes. These changes affect not

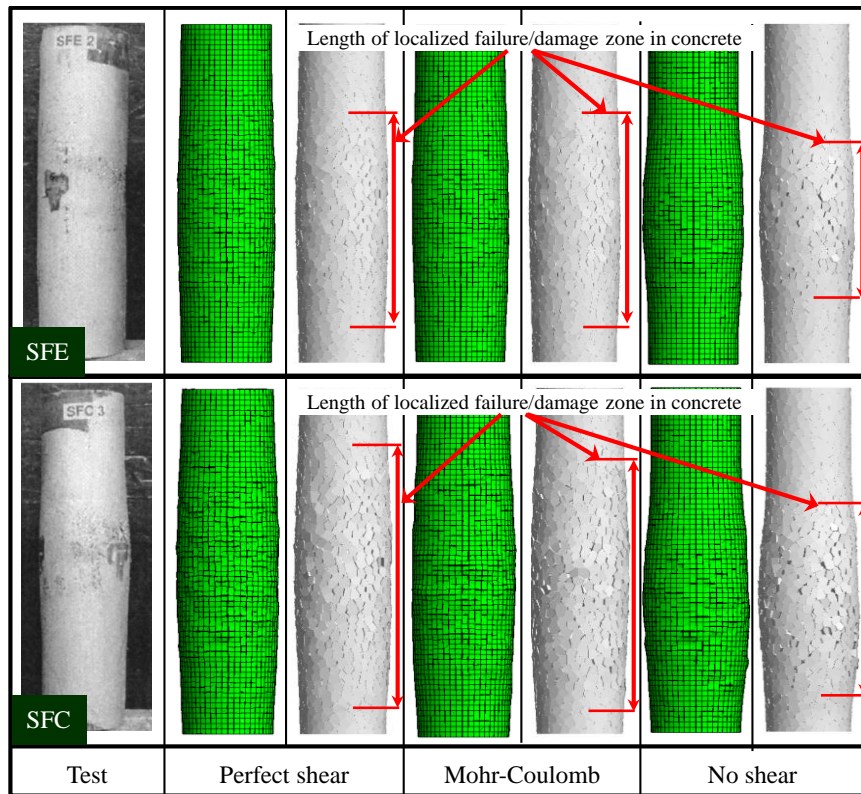


Fig.8 Comparison of deformed behavior for SFE and SFC (magnification x 1)

only the axial resistance of the composite but also its structural behavior. In both the SFE and SFC cases, the perfect shear case showed the highest prediction of axial resistance which overestimates the test results by at least 35%. On the other hand, in cases where shear resistance is neglected, localization of damage tends to occur for both SFE and SFC specimen. This localized damage or failure behavior is more evident in SFC specimen which also showed a softening post-peak response. Of note is the increased in the peak strength of the no shear case for SFC specimen which is likely due to the increased in confinement pressure. This behavior was documented by Orito et al. [13] in their experiments of concrete-only loaded specimen which showed that when a lower bond between the concrete and steel tube exists, the confinement pressure in concrete is also increased resulting to increased axial resistance of the composite. The results also show that the presence of bond provides a more distributed damage while the lack of it results to a localized failure. This can be observed from almost identical deformed behavior of the perfect shear case and the Mohr-Coulomb case for both SFE and SFC specimens. In all the cases considered, the Mohr-Coulomb friction model provides the best estimate of both strength prediction and deformed behavior of the subject CFSTs. The model showed that it is sufficient in simulating the mechanism of concrete-steel tube interaction in CFST. This condition was satisfied both for concrete-only loaded, and concrete and steel loaded cases.

## 7. COMPARISON WITH OTHER EXPERIMENTS

To further determine the applicability of the

investigated Mohr-Coulomb friction interface, the model was utilized in the simulation of uniaxial compression tests performed by O'Shea and Bridge [14], and Lai and Ho [15]. Table 2 shows the properties of these specimens. The results from these simulations are shown in Fig. 9. The reported axial strains from test results were all based on LVDT measurements while the reported axial loads were obtained directly from the compression machine readings. The axial load-strain results shown in Fig. 9 confirm that the use of the Mohr-Coulomb friction case for the proposed coupled RBSM-shell FEM method is a sufficient interface model as it provides a good prediction of initial stiffness and CFST peak strength both for CFST loaded only in concrete (i.e., S30CL50C) and those loaded in steel and concrete (i.e., S10CS50A, CN0-114-30, and CN0-114-80). Also, the model was able to predict the axial strains at peak load quite reasonably.

Table 2 Properties of simulated specimens (B)

Type	H (mm)	D (mm)	T (mm)	f'c (MPa)	fy (MPa)	Loaded section
SC1	659	190	0.86	41	211	CS
SC2	571	165	2.82	56.4	363	C
SC3	350	112	0.96	31.4	313	CS
SC4	350	112	0.96	79.9	317	CS

\*SC1 = S10CS50A; \*SC2= S30CL50A; SC3 = CN0-1-114-30; SC4 = CN0-1-114-80. CS = concrete and steel; C = concrete; H = height; D = diameter; T = steel tube thickness; f'c = concrete's compressive strength; and fy = yield strength of steel tube.

In addition, both softening and hardening behavior observed in the test results were also well simulated by the said model.

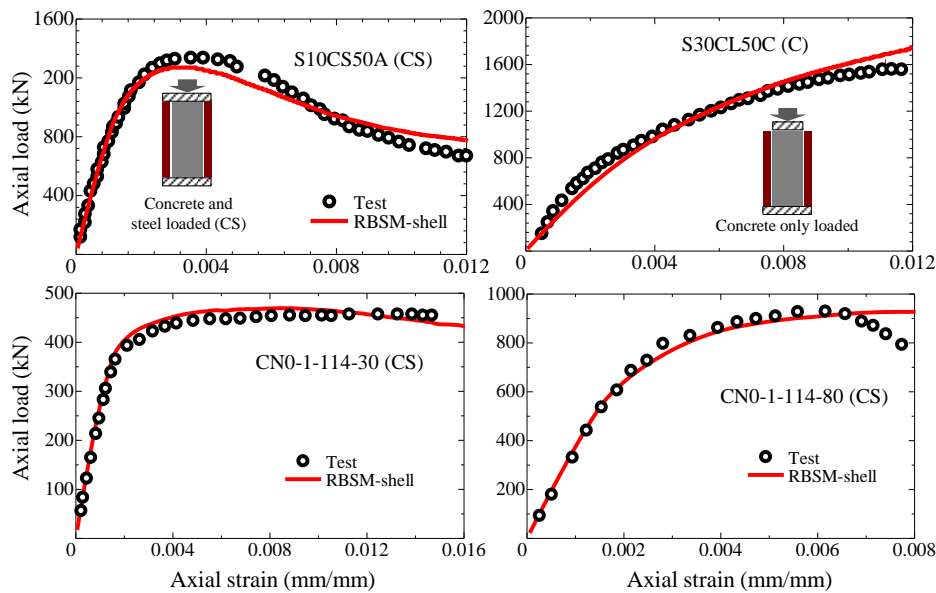


Fig.9 Comparison of axial load-displacement curves between test and simulation results

## 8. CONCLUSIONS

The paper investigated three types of numerical approach, which consist of perfect shear case, Mohr-Coulomb friction case, and no shear case, for modeling concrete-steel interface in CFST. It was showed that among the models considered, the Mohr-Coulomb friction case is the most appropriate interface model based on performed quantitative and qualitative comparisons utilizing two types of axial load applications. The said model was further validated with axial load-strain curves from other experiments and the results were also found in good agreement. Considering further work, it is desirable to improve the contact algorithm between the RBSM and shell to reduce the effect of mesh-size ratio and to provide a more intuitive definition of contact area.

## REFERENCES

- [1] Viridi, K. S., and Dowling, P. J., "Bond Strength in Concrete Filled Steel Tubes." IABSE, Periodical, 1980, 125-139.
- [2] Roedner, C.W., Cameron B., and Brown, C.B., "Composite Action in Concrete Filled Tubes," J. of Struct. Eng., 1999, 125(5), 477-484.
- [3] Hu, H.T., Huang, C.H., and Wu, M.H., "Nonlinear Analysis of Axially Loaded Concrete-Filled Tube Columns with Confinement Effect," J. Struct. Eng., 2003, 129(10):1322-1329.
- [4] Johansson M., Gylltoft, K., "Mechanical Behavior of Circular Steel-Concrete Composite Stub Columns," J. Struct. Eng., 2002, 128(8):1073-1081.
- [5] Yamamoto, Y. et al., "Crack propagation analysis of reinforced concrete wall under cyclic loading using RBSM," European Journal of Environmental and Civil Eng., 18(7), 2014, 780-792
- [6] Kawai, T., "New discrete models and their application to seismic response analysis of structures," Nuclear Eng. and Design, 1978, 48:207-229.
- [7] Qiao, D. et al., "Crack patterns of concrete with single rebar subjected to non-uniform and localized corrosion." J. of Construction and Building Materials, 116(2016), 366-377.
- [8] Gedik Y. H. et al., "Evaluation of Three Dimensional Effects in Short Deep Beams using a Rigid Body Spring Model," Cement and Concrete Composites. 33-978-991.
- [9] Yamamoto, Y., Okazaki S., and Nakamura H., "Crack propagation and local failure simulation of reinforced concrete subjected to projectile impact using RBSM." Proc., 35th Intl. Conf. on Ocean, Offshore and Arctic Eng. 2016, Busan, South Korea.
- [10] Yamamoto, Y. et al., "Analysis of compression failure of concrete by three-dimensional rigid body spring model," Doboku Gakkai Ronbunshuu E, 64, 2008, 612-630. [in Japanese].
- [11] Noguchi, H., and Hisada, T., "Integrated FEM Formulation for Total/Updated-Lagrangian Method in Geometrically Nonlinear Problems," JSME Intl. Journal, 1995, Se. A, Vol. 38, No.1.
- [12] Sze, KY., Liu XH., Lo, SH., "Popular benchmark problems for geometric nonlinear analysis of shells," Finite Elements in Analysis and Design, 2004, 40: 1551-1569.
- [13] Orito, Y. et al., "Study on the unbounded steel tube concrete structures," Proc., Eng. Foundation Conf. on Composite Constructions, 1987, Henniker, N.H.
- [14] O'shea M.D., Bridge, R.Q., "Design of Circular Thin-walled Concrete Filled Steel Tubes," J. Struct. Eng., 2000, 126(11):1295-1303.
- [15] Lai, M.H. and Ho, J.C.M., "Axial strengthening of thin-walled concrete-filled steel tube columns by circular jackets," Thin-Walled Structures, 97, 2015, 11-21.